J Mater Sci (2008) 43:1568–1575
DOI 10.1007/s10853-007-2326-y

The strain rate and temperature dependence of microstructural evolution of Ti–15Mo–5Zr–3Al alloy

Woei-Shyan Lee · Chi-Feng Lin · Tao-Hsing Chen · Hsin-Hwa Hwang

Received: 9 April 2007 / Accepted: 15 November 2007 / Published online: 31 December 2007

Abstract A compressive split-Hopkinson pressure bar apparatus and transmission electron microscopy (TEM) are used to investigate the deformation behaviour and microstructural evolution of Ti–15Mo–5Zr–3Al alloy deformed at strain rates ranging from 8×10^2 s^{-1} to 8×10^3 s^{-1} and temperatures between 25 °C and 900 °C. In general, it is observed that the flow stress increases with increasing strain rate, but decreases with increasing temperature. The microstructural observations reveal that the strengthening effect evident in the deformed alloy is a result, primarily, of dislocations and the formation of α phase. The dislocation density increases with increasing strain rate, but decreases with increasing temperature. Additionally, the square root of the dislocation density varies linearly with the flow stress. The amount of α phase increases with increasing temperature below the β transus temperature. The maximum amount of α phase is formed at a temperature of 700 °C and results in the minimum fracture strain under the current loading conditions.

Introduction

Titanium alloys are characterized by a high strength-to-weight ratio, excellent corrosion resistance and good formability. Consequently, such alloys are commonly used in applications requiring light-weight, chemically-inert components. In the mid-1980s, α+β phase Ti–6Al–4V was commonly regarded as an ideal material for medical implants [1–2]. However, recent research has revealed that Ti–6Al–4V debris contains Group V chemical elements, which are harmful to human health [3]. Accordingly, researchers have shown increasing interest in the potential of β phase Ti–15Mo–5Zr–3Al for medical applications [4–5]. In general, this alloy is known to have good biocompability characteristics and favourable mechanical properties. However, its dynamic mechanical behaviour under the high strain rate and temperature conditions experienced during typical manufacturing processes, e.g. forging and machining, are poorly understood. As a result, the precise shape and mechanical properties of manufactured Ti–15Mo–5Zr–3Al alloy components are not easily predicted. Hence, a requirement exists to investigate the deformation behaviour of Ti–15Mo–5Zr–3Al alloy under high strain rate loading conditions over a wide temperature range.

It is recognized that the variations observed in the stress–strain curves of impacted specimens are related to the microstructural evolution of the deformed material. Accordingly, observations of the deformed microstructures of impacted specimens can provide useful insights into the strengthening mechanisms and plastic deformation behaviour of materials subject to deformation under different strain rate and temperature conditions. Dislocation slip is known to have a major effect on the flow stress curves of plastically deformed materials. Under high strain rate loading conditions, the rapid multiplication of dislocations suppresses the dislocation slip phenomenon and induces a strengthening effect [6–7]. However, under high temperature deformation conditions, the increased temperature not only increases the annihilation of dislocations, but also

W.-S. Lee (✉) · T.-H. Chen · H.-H. Hwang
Department of Mechanical Engineering, National Cheng Kung University, Tainan 701, Taiwan
e-mail: wslee@mail.ncku.edu.tw

C.-F. Lin
National Center for High-Performance Computing, Hsin-Shi, Tainan County 744, Taiwan

provides the dislocations with additional energy to overcome short-range barriers. As a result, a work-softening effect is observed. Thus, it is apparent that the strain rate and the temperature exert opposing effects on the mechanical response of engineering materials. Since Ti–15Mo–5Zr–3Al alloy is a metastable, β-phase alloy, a strengthening effect is provided by the precipitation of α phase following solution treatment at temperatures lower than the β transus temperature (785 °C) [8]. Accordingly, previous researchers have proposed several thermal treatments designed specifically to control the features and amount of precipitated α phase in order to enhance the mechanical response of Ti–15Mo–5Zr–3Al alloy [9–11]. In general, the mechanical response of Ti–15Mo–5Zr–3Al alloy components is significantly dependent on both the strain rate and temperature conditions encountered during their manufacture or subsequent service lives. Consequently, it is essential to systematically examine the correlation between the mechanical properties of Ti–15Mo–5Zr–3Al alloy and its microstructural evolution over a range of strain rate and temperature loading conditions.

Accordingly, this study employs a compressive split-Hopkinson pressure bar (SHPB) apparatus to investigate the deformation response of Ti–15Mo–5Zr–3Al alloy under strain rates between 8×10^2 s^{-1} and 8×10^3 s^{-1} and temperatures ranging from 25 °C to 900 °C. The microstructural evolution of the deformed specimens is observed via transmission electron microscopy (TEM), with particular focus placed on the effects of strain rate and temperature on the formation and slip of dislocations and the extent of α-phase precipitation. Finally, the correlation between the microstructural evolution characteristics and the macro-mechanical response of the deformed specimens is systematically analysed and discussed.

Experiments

The Ti–15Mo–5Zr–3Al alloy tested in this study was solution-treated at a temperature of 735 °C for 0.5–1 h and was then aged at 425–500 °C for 17 h. The chemical composition (wt.%) of the alloy was as follows: 15%Mo, 5.2%Zr, 2.9%Al, 0.35%Fe, 0.05%N, 0.20%O, 0.02%H and a balance of Ti. Rods with a diameter of 25 mm and a length of 170 mm were formed in a drawing process and cylindrical specimens with a diameter and height of 7 mm were then machined using an electro-discharge machine (EDM). The specimen surfaces were carefully ground to assure a close contact between the specimen and the pressure bars of the SHPB apparatus during impact testing.

The Ti–15Mo–5Zr–3Al specimens were compression-tested at strain rates of 8×10^2 s^{-1}, 3×10^3 s^{-1} and 8×10^3 s^{-1} and temperatures of 25 °C, 300 °C, 500 °C, 700 °C and 900 °C. The striker, incident and transmitter bars of the SHPB apparatus were fabricated of DC 53 high-strength tool steel and had a diameter of 12.7 mm. The SHPB apparatus and experimental procedures are well documented by Lindholm in [12]. For the compression tests performed at temperatures of 300 °C, 500 °C, 700 °C and 900 °C, the specimens were enclosed in a clamshell radiant-heating furnace with an internal diameter of 25 mm and a heating element of length 300 mm. The specimen temperature was monitored using a K-type (chromel–alumel) thermocouple positioned in contact with the specimen surface. Prior to impact testing, the specimen and the two ends of the pressure bars holding the specimen were maintained at the required test temperature for a duration of approximately 10 min to ensure a uniform temperature distribution at the specimen/pressure bar interface. The resulting temperature gradient induced along the lengths of the two pressure bars is known to affect both the elastic modulus of the bars and the propagation velocity of the pressure pulse. Accordingly, it is necessary to modify the original equations for the strain, strain rate and stress of the deformed specimens. The necessary modifications are summarized by Chiddister and Malvern in [13] and by the current authors in [14].

Following impact testing, the microstructures of the deformed specimens were observed via TEM in order to investigate the respective effects of strain rate and temperature on the formation of dislocations and the precipitation of α phase. The thin foils required for the TEM observations were prepared by cutting slices of 0.7 mm thickness from the centre of the deformed specimens perpendicular to the compression axis using a diamond-bladed cutting machine. The slices were ground with 600 grit paper to a thickness of 0.2 mm, and discs with a diameter of 3 mm were then removed using a spark cutter. The discs were electro-polished in a twin-jet polishing machine using a solution of Methanol (500 mL), I-Butanol (300 mL) and Perchloric acid (50 mL) at 25 °C and a 20 V DC voltage. Finally, the electro-polished disks were ion-milled by argon in a Gatan PIPS-691 Ion-Miller with an accelerating voltage of 4.5 keV and a beam glancing angle of 4°. The specimens were then examined using a JEOL TEM-3010 analytical scanning transmission electron microscope with an operating voltage of 300 kV.

Results and discussions

Stress–strain curves

Figure 1a–c present the stress–strain curves of Ti–15Mo–5Zr–3Al alloy deformed at strain rates of 8×10^2 s^{-1}, 3×10^3 s^{-1} and 8×10^3 s^{-1}, respectively, at temperatures

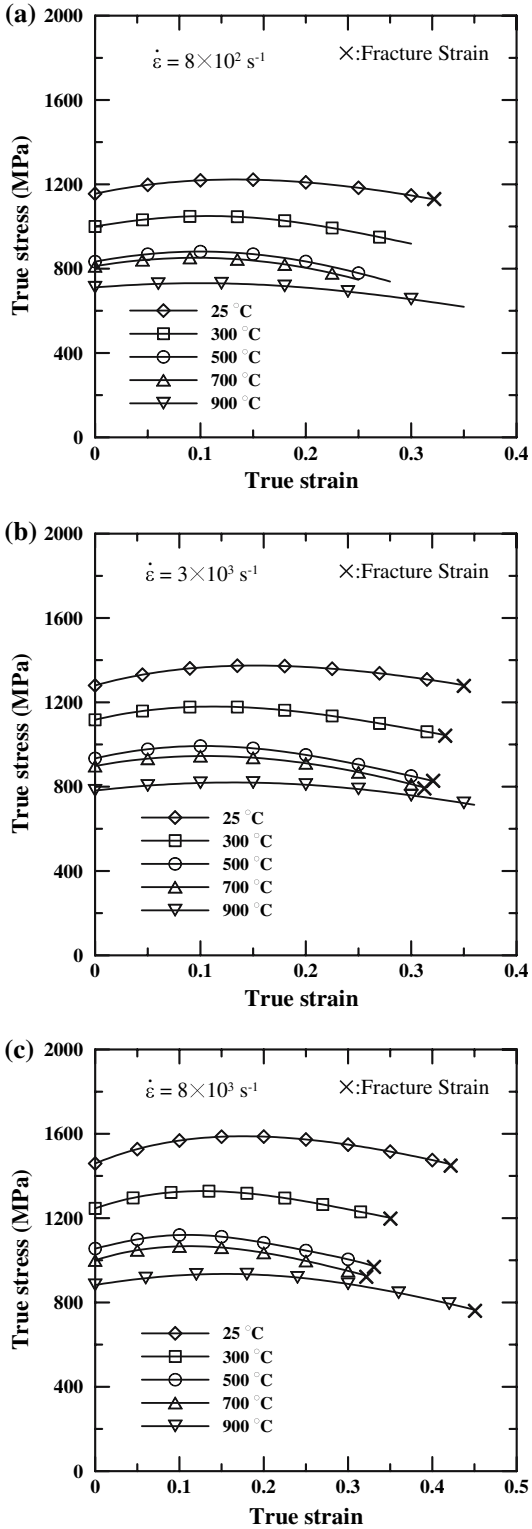

Fig. 1 True stress–strain curves of Ti–15Mo–5Zr–3Al alloy deformed at various temperatures under strain rates of (**a**) 8×10^2 s^{-1}; (**b**) 3×10^3 s^{-1}; and (**c**) 8×10^3 s^{-1}

between 25 °C and 900 °C. In general, it is observed that the flow stress increases with increasing strain rate, but decreases with increasing temperature. It can also be seen that for a constant strain rate, the flow stress increases with increasing strain initially, but then reduces as the strain is increased further. Table 1 summarizes the yield stress, fracture strain and maximum stress for each of the current specimens. The results show that the yield stress and the maximum stress both increase with increasing strain rate, but decrease with increasing temperature. At the lowest strain rate of 8×10^2 s^{-1}, the specimen fractures only at a deformation temperature of 25 °C. However, when the strain rate is increased to 8×10^3 s^{-1}, the specimens all fracture, irrespective of the temperature conditions. Hence, the results show that Ti–15Mo–5Zr–3Al alloy fractures more readily at higher strain rates or at lower temperatures. Table 1 also shows that for a constant temperature, the fracture strain increases with increasing strain rate, which suggests that the fracture toughness of the alloy is enhanced at higher strain rates. Finally, it is observed that for a given strain rate, the fracture strain reduces with increasing temperature at temperatures lower than 700 °C, but increases significantly at a deformation temperature of 900 °C. This tendency implies that an increasing deformation temperature is accompanied by a significant change in the Ti alloy microstructure, particularly at temperatures between 700 °C and 900 °C.

Microstructural observations

The macro-mechanical behaviour of the deformed Ti–15Mo–5Zr–3Al alloy specimens is closely related to the microstructural changes induced by the applied strain rate and temperature loading conditions. Figures 2 and 3 present diffraction patterns and TEM micrographs of the Ti alloy deformed at a true strain of 0.2 and various strain rate/temperature conditions. The diffraction patterns in Fig. 2a, b reveal the presence of elongated α phase within the β matrix of the Ti alloy deformed at 25 °C. Note that the diffraction patterns in Fig. 2a, b are taken from the selected area by white squares C and D in Fig. 2c, respectively. The micrographs presented in Fig. 2c–f and Fig. 3a–f reveal that the dislocation density increases with increasing strain rate, but decreases with increasing temperature. Furthermore, it can be seen that the amount of α phase (as indicated by white arrow in Fig. 3a–d) increases with increasing temperature at temperatures lower than 700 °C. Observing the dislocation structures, it is found that the dislocation cells are large and have thin walls (as indicated by arrow A) composed of tangled dislocations (as indicated by arrow B) in the specimen deformed at a strain rate of 8×10^2 s^{-1} and a temperature of 25 °C (see Fig. 2c). However, for the same deformation temperature, when the strain rate is increased to 8×10^3 s^{-1}, the dislocation cell size reduces and the cell walls (as indicated by arrow A) become thicker (see Fig. 2d). Under this higher strain rate condition, the

Table 1 Yield stress, maximum stress and fracture strain in Ti–15Mo–5Zr–3Al alloy deformed at strain rates of 8×10^2 s^{-1}, 3×10^3 s^{-1} and 8×10^3 s^{-1} and temperatures ranging from 25 °C to 900 °C

Temperature (°C)	Strain rate (s^{-1})	Yielding stress (MPa)	Fracture strain	Max. stress (MPa)
25	8.0×10^2	1,155	0.32	1,223
	3.0×10^3	1,280	0.35	1,374
	8.0×10^3	1,459	0.42	1,588
300	8.0×10^2	1,000	–	1,050
	3.0×10^3	1,117	0.33	1,180
	8.0×10^3	1,246	0.35	1,328
500	8.0×10^2	833	–	881
	3.0×10^3	934	0.32	993
	8.0×10^3	1,055	0.33	1,121
700	8.0×10^2	811	–	852
	3.0×10^3	898	0.30	945
	8.0×10^3	1,000	0.32	1,067
900	8.0×10^2	711	–	731
	3.0×10^3	781	–	820
	8.0×10^3	883	0.45	935

dislocation density increases, and the greater number of dislocations tangled at the cell walls suppress dislocation movement. In other words, as the number of tangled dislocations within the cell wall increases, the force required for the dislocations to overcome the barriers formed by these tangled dislocations also increases. Correlating the stress–strain curves in Fig. 1 with the increased dislocation density observed at higher strain rates in Fig. 2d, it can be inferred that the flow stress increases with increasing dislocation density. However, Fig. 2e, f suggest that the presence of α phase in the matrix also contributes to the strengthening effect observed in the deformed alloy at temperatures lower than 700 °C. Specifically, the α phase presents a barrier to dislocation movements, causing the dislocations to pile up at the phase boundary. It seems reasonable to assume that the amount of precipitated α phase has a direct effect on the mechanical behaviour of the Ti–15Mo–5Zr–3Al alloy. As the deformation temperature is increased, the thermal activation energy of the dislocations is also increased, and hence their ability to overcome short-range barriers is enhanced. Therefore, at a strain rate of 8×10^2 s^{-1} and a temperature of 300 °C, the dislocation cells have a looser structure (as indicated by arrows A and B in Fig. 2e) and the dislocation density is reduced. Furthermore, a greater amount of α phase is precipitated (see Fig. 2e). However, for the same deformation temperature, but an increased strain rate of 8×10^3 s^{-1}, both the dislocation density and the cell wall thickness (as indicated by arrows A and B) are increased (see Fig. 2f).

At higher temperatures of 500 °C and 700 °C, the number of dislocations decreases. At a strain rate of 8×10^2 s^{-1}, dislocation multiplication restrained because the dislocation annihilation caused by the temperature rise, i.e. thermal softening effect, was stronger than the dislocation multiplication caused by the imposed strain rate, i.e. work hardening rate effect. At the aforementioned strain rate, the dislocation density at deformation temperatures of 500 °C and 700 °C is lower than that observed at 25 °C and 300 °C, as shown in Fig. 3a, c from which fewer dislocations and no cell substructures are found since the dislocation annihilation dominates the deformation process. However, at a higher strain rate of 8×10^3 $s^{-1}$and at the deformation temperatures of 500 °C and 700 °C, the annihilation of dislocation substructure did not occur because dislocation multiplication induced by the enhancement of strain rate was more evident than the dislocation annihilation caused by the temperature rise which, in turn, leads to an increase in dislocation density. As a result, large dislocation and cell structures were still formed, as shown in Fig. 3b, d, respectively. Comparing the cell substructures formed at a strain rate of 8×10^3 s^{-1} in Figs. 2d, f and 3b, d, it is apparent that the cell size increases and the cell walls become thinner as the temperature is increased. Furthermore, comparing Figs. 2e and 3a, c at a strain rate of 8×10^2 s^{-1}, it is observed that the amount of α phase precipitated in the β matrix at 500 °C and 700 °C is greater than that formed at 300 °C. The increased amount of α phase increases the resistance to dislocation movements and causes a greater accumulation of tangled dislocations at the α phase boundary. Accordingly, plastic deformation is suppressed, and the mechanical strength of the alloy is increased. It is thought that the presence of α phase in the matrix dominates the high temperature strength characteristics of Ti–15Mo–5Zr–3Al alloy at temperatures lower than the β transus temperature, i.e. 785 °C. However, at higher temperatures, e.g. 900 °C, the microstructures of the specimens deformed at strain rates of 8×10^2 s^{-1} and 8×10^3 s^{-1} contain

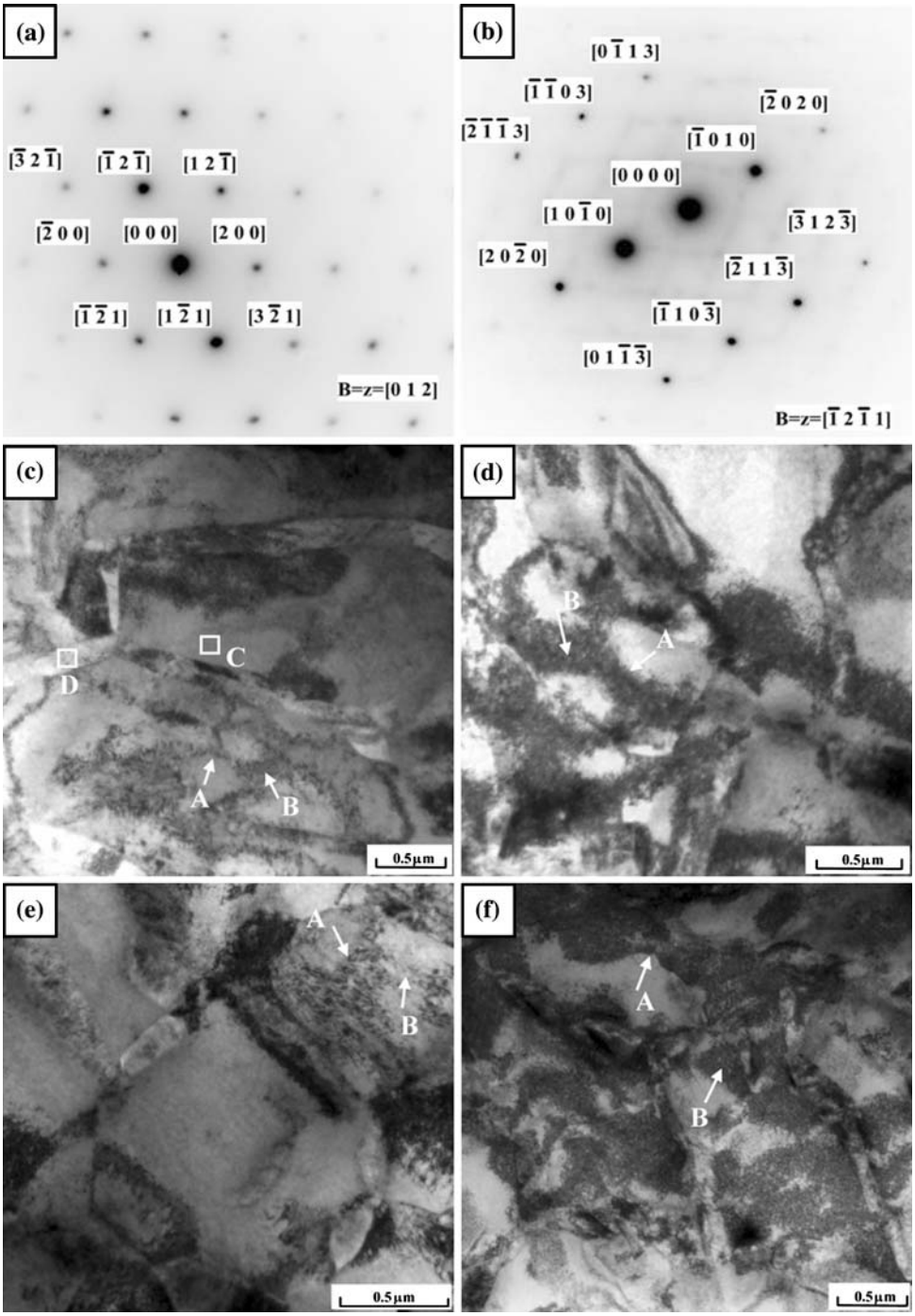

Fig. 2 Selected area electron diffraction patterns of: (**a**) β matrix and (**b**) α phase. Dislocation substructure and α phase precipitation in specimens deformed at true strain of 0.2 and loading conditions of: (**c**) 25 °C, $8 \times 10^2\ s^{-1}$; (**d**) 25 °C, $8 \times 10^3\ s^{-1}$; (**e**) 300 °C, $8 \times 10^2\ s^{-1}$; (**f**) 300 °C, $8 \times 10^3\ s^{-1}$ (arrow A: dislocation wall; arrow B: dislocation tangles)

subgrains and a very low number of dislocations (see Fig. 3e, f, respectively). Furthermore, because the temperature is higher than the β transus temperature, the β matrix contains no α phase. The combined effects of thermal activation assistance at higher deformation temperatures and the absence of α phase reduce the intensity of the driving force required to produce dislocation movements, and hence the flow stress reduces considerably at temperatures ranging from 700 °C to 900 °C, as evidenced in Fig. 1.

Quantitative analysis of dislocation density and α phase

The correlation between the microstructural evolution of the Ti–15Mo–5Zr–3Al alloy and its macromechanical response can be quantified by measuring the dislocation density and the amount of α phase within the matrix. In this study, the dislocation density, ρ, was determined using the analytical formula proposed by Ham [15], i.e. $\rho = 2N/Lt$, where n is the number of intersections between a dislocation and a random set of lines of length

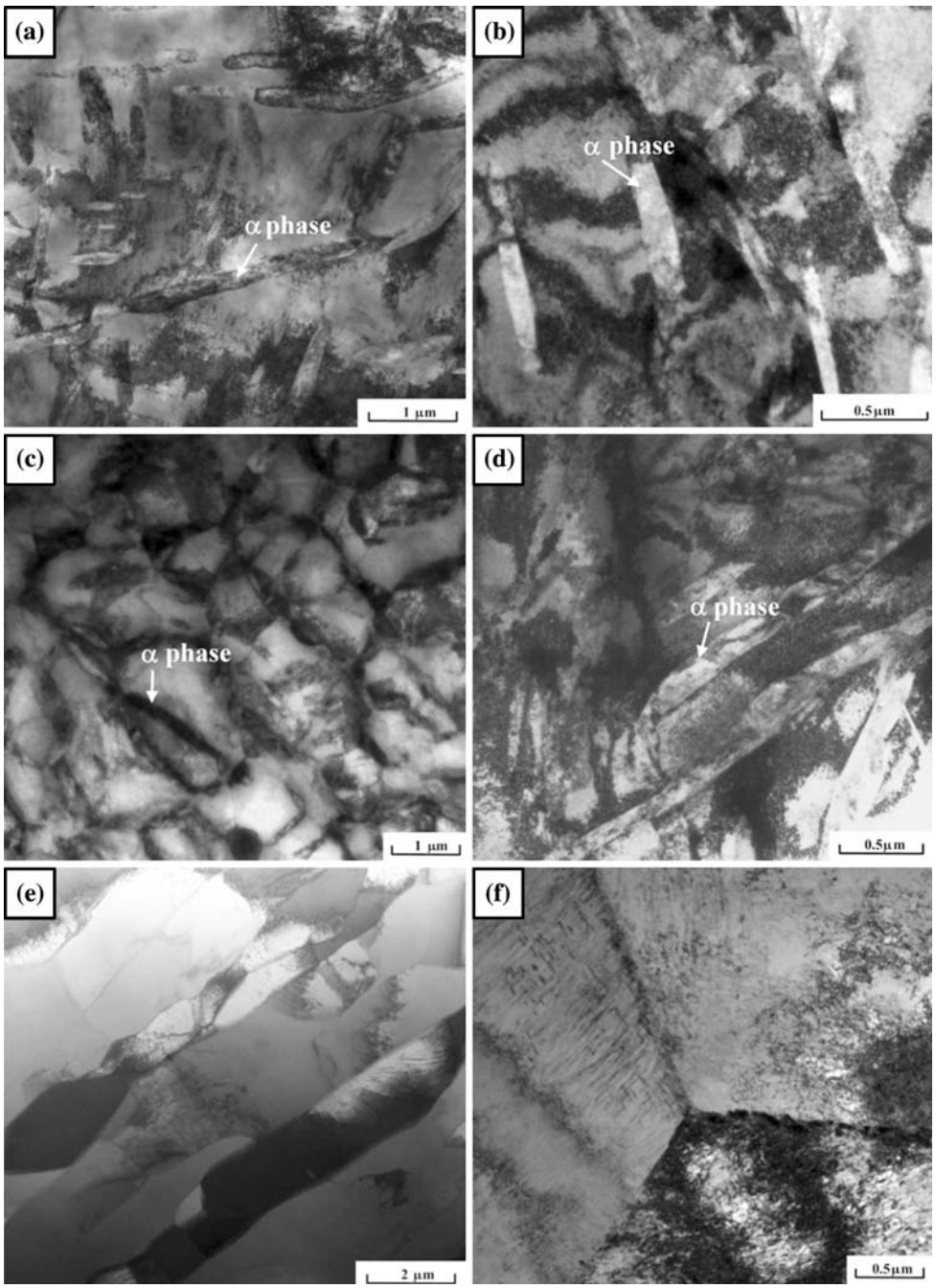

Fig. 3 Dislocation substructure and α phase precipitation in specimens deformed at true strain of 0.2 and loading conditions of: (**a**) 500 °C, 8×10^2 s^{-1}; (**b**) 500 °C, 8×10^3 s^{-1}; (**c**) 700 °C, 8×10^2 s^{-1}; (**d**) 700 °C, 8×10^3 s^{-1}; (**e**) 900 °C, 8×10^2 s^{-1}; (**f**) 900 °C, 8×10^3 s^{-1}

L, and t is the foil thickness. In the current analysis, the dislocation density was calculated for the specimens deformed at a strain of 0.2 under each of the current strain rate/temperature conditions. Figure 4 reveals that the square root of the dislocation density increases linearly with the flow stress, which implies that the combined effect of the strain rate and the temperature determines the correlation between the dislocation density and the flow stress. Quantitative measurements of the amount of α phase precipitated in the β matrix were obtained via X-ray diffraction. Figure 5 presents the X-ray diffraction profiles of the Ti–15Mo–5Zr–3Al alloy deformed at temperatures ranging from 25 °C to 900 °C at a constant strain rate of 8×10^3 s^{-1}. It can be seen that peaks corresponding to α phase $(10\bar{1}1)$ are present only in the profiles corresponding to temperatures of 700 °C or lower, and are particularly strong at temperatures of 500 °C and 700 °C. The amount of α phase in the β matrix was estimated quantitatively by computing the α phase intensity, I_α, in accordance with the expression [16]

$$I_\alpha = I\{10\bar{1}1\}_\alpha / I\{200\}_\beta, \tag{8}$$

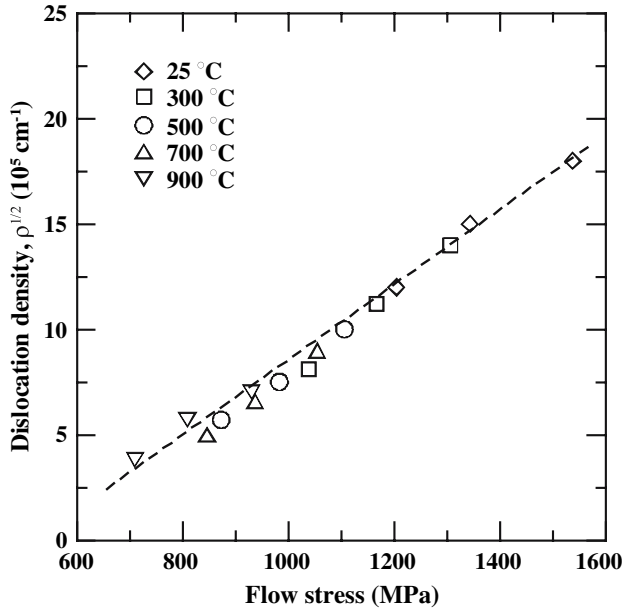

Fig. 4 Variation of square root of dislocation density as function of flow stress

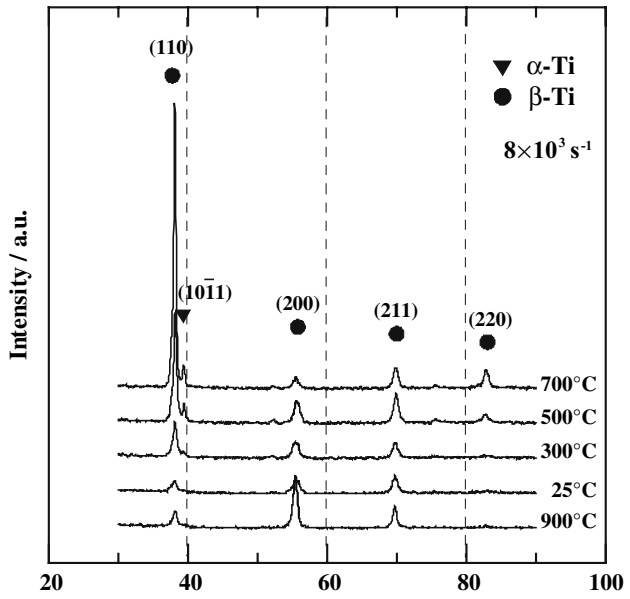

Fig. 5 X-ray diffraction profiles of Ti–15Mo–5Zr–3Al alloy deformed at $8 \times 10^3 s^{-1}$ and temperatures ranging from 25 °C to 900 °C

where $I\{200\}_\beta$ is the base reflection intensity, i.e. the intensity of the pure β matrix.

Figure 6 plots the variations of the dislocation density, the α phase intensity and the flow stress with the deformation temperature as a function of the strain rate. The results show that for a given strain rate, the flow stress and the dislocation density decrease as the temperature increases. It

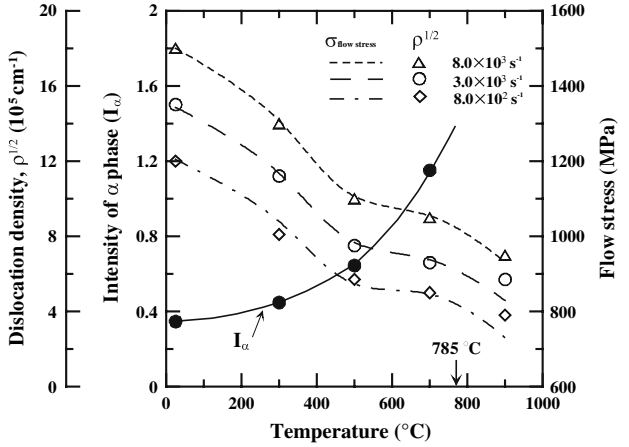

Fig. 6 Variation of dislocation density, α phase intensity and flow stress with temperature as function of strain rate

is also observed that the intensity of the α phase increases with increasing temperature below the β transus temperature. It is thought that the precipitated α phase not only imposes barriers to dislocation motion, but also acts as the origin of dislocation multiplications. Therefore, an increased amount of α phase induces the generation of additional dislocations and leads to an obvious softening resistance effect (particularly at 700 °C).

Figure 7 shows that the fracture strain decreases with an increasing amount of α phase at temperatures lower than 700 °C. The microstructural observations presented in Figs. 2 and 3 reveal that the formation of α phase causes the accumulation of dislocations at the phase boundaries, resulting in extreme stress concentrations. Thus, cracks form more readily within the microstructure as the amount

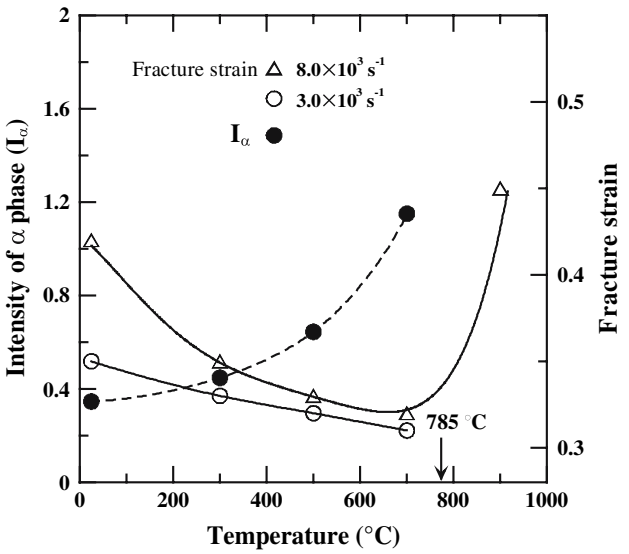

Fig. 7 Variation of α phase intensity and fracture strain with temperature as function of strain rate

of α phase increases, and hence the fracture strain reduces. However, at temperatures higher than the β transus temperature, α phase is not precipitated in the matrix, and hence the fracture strain increases.

Conclusions

This study has investigated the effects of strain rate and temperature on the dynamic deformation response and microstructural evolution of Ti–15Mo–5Zr–3Al alloy. In general, the results have shown that the flow stress increases with increasing strain rate, but decreases with increasing temperature. The microstructural observations have shown that the dislocation density and the amount of precipitated α phase have a significant effect on the dynamic plastic deformation of the Ti–15Mo–5Zr–3Al alloy. Dislocation generation is enhanced at higher strain rates, but is suppressed at higher deformation temperatures. Furthermore, the square root of the dislocation density increases linearly with increasing flow stress. The amount of precipitated α phase is insensitive to the strain rate, but increases with increasing temperature at temperatures lower than the β transus temperature. The presence of α phase provides a strengthening effect since it assists in the generation of dislocations and suppresses their movement. However, significant stress concentrations are formed at the boundaries of the α phase, which result in the formation of cracks within the matrix. Hence, the fracture strain reduces as the amount of α phase increases.

Acknowledgements The authors gratefully acknowledge the financial support provided to this study by the National Science Council (NSC) of Taiwan under contract No. NSC-93-2212-E006-076. Particular appreciation is also extended to Kobe Steel Ltd., Japan, for their supply of the Ti–15Mo–5Zr–3Al alloy bars.

References

1. Steinemann SG (1984) Ti Sci Tech 2:1327
2. Dobbs HS, Scales JT (1983) In: ASTM. Philadelphia, 1983, p 173
3. Nichols KG, Puleo DA (1997) J Biomed Mater Res 35:256
4. Katsuhiko M, Kenji D, Tomiharu M, Yoshio S (2002) Mater Trans 43:2936
5. Kim HM, Takadama H, Kokubo T, Nishiguchi S, Nakamura T (2000) Biomaterials 21:353
6. Murr LE (1978) Scripta Mater 12:201
7. Lee WS, Shyu JC, Chiou ST (2000) Scripta Mater 42:51
8. Boyer R, Welsch G, Collings EW (1994) In: Materials properties handbook: Titanium alloys. Materials Park, ASM International
9. Ikeda M, Komatsu SY, Sugimoto T, Hasegawa M (1998) Mater Sci Eng A 243:140
10. Komatsu Shin-ya, Ikeda M, Sugimoto T, Kamei K, Maesaki O, Kojima Masa-aki (1996) Mater Sci Eng A 213:61
11. Ikeda M, Komatsu Shin-ya, Sugimoto T, Hasegawa M (1998) Mater Sci Eng A 243:140
12. Lindholm US, Yeakly LW (1968) Exp Mech 8:1
13. Chiddister JL, Malvern LE (1963) Exp Mech 3:81
14. Lee WS, Lin CF (1998) Mater Sci Eng A 241:48
15. Ham RK (1961) Philos Mag 6:1183
16. Nishimura T, Nishigaki M, Moriguchi Y (1982) R&D Technical report, Kobe Steel, vol 32, p 52